Boukhellouf *et al.*
*European Transport Research Review* (2023) 15:12
https://doi.org/10.1186/s12544-023-00586-1

European Transport Research Review

ORIGINAL PAPER

Open Access

# Merging and diverging operations: benchmark of three European microscopic simulation tools and comparison with analytical formulations

Mathis Boukhellouf[1*], Christine Buisson[1] and Nicolas Chiabaut[2]

## Abstract

**Purpose** We benchmark three European microscopic simulation software's ability to reproduce congested patterns at merges and diverges by comparing their macroscopic outputs to validated analytical formulations. The capacity drop and, in the specific case of merges, the priority ratio are assessed. At the microscopic scale, the spatial distribution of lane changes at merges is examined.

**Method** A single reference state is built for all three simulation tools. A point-based diverge and an extended merge are reproduced in the simulation tools. Under traffic conditions ranging from free-flow to congestion, vehicles counts and vehicles trajectories are collected to compute the selected indicators, which help to conclude for the considered reference state.

**Results** The considered simulation tools correctly reproduce the merges and diverges elementary behaviors. However, their default configuration does not, entirely or partially, reproduce the traffic conditions induced by insertions and desertions as predicted by the analytical models.

**Discussion** The study could be enriched by including the benchmark of other simulation tools. In addition, the networks studied are elementary and may not reflect completely the traffic situations encountered on the highways.

**Keywords** Traffic flow, Traffic microscopic simulation tools, Benchmark, Merges, Diverges, Capacity drop, Mandatory lane changes

*Correspondence:
Mathis Boukhellouf
mathis.boukhellouf@entpe.fr
[1] LICIT- Éco7, École nationale des travaux publics de l'État & Université Gustave Eiffel, 3 rue Maurice Audin, 69120 Vaulx-en-Velin, France
[2] Département de la Haute-Savoie, Direction des Nouvelles Mobilités, 1 rue du 30ème Régiment d'Infanterie, 74000 Annecy, France

## 1 Introduction

Engineers and public authorities use microscopic simulation tools to anticipate and evaluate traffic scenarios on specific networks [1–5]. Hence, such projects can be pre-assessed before deployment on the field, thus limiting the risk of providing an inadequate answer to the network situation. Discontinuities like on-ramps, where traffic streams merge, and off-ramps, where traffic streams diverge, often enmesh a network of highways. They may act as active bottlenecks, inducing capacity drops and more delays for passengers [6–9]. Moreover, streams and lane management have been changing priorities in recent years. Traffic managers now deal with heterogeneous streams, as shows the emergence of connected and automated vehicles [10, 11], or with the dynamic management of lanes, as shows the planning of high-occupancy vehicle (HOV) lanes projects in Europe [12]. These new priorities raise the question of interfaces, which deal with merging heterogeneous streams or weaving flows induced by special lanes activation, the latter relying on a coupled merging and diverging behavior [13]. Thus, simulation tools must reproduce correctly the complex phenomena characterizing merge and diverge operations to reliably estimate flows or time losses induced by these discontinuities.

Many traffic microscopic simulation tools are available nowadays; see [14, 15] for a review. Therefore, choosing the most suitable for one given traffic criterion is difficult [16, 17]. A benchmark approach, aiming at comparing the outputs of these tools for a test scenario, seems necessary, thus, to assess their correct operation concerning this criterion [16, 18]. This critical approach would also ensure the quality of the simulation tool used with its ability to reproduce the on-field observed conditions [4, 19, 20]. Authors calling for a benchmark approach first proposed one that compares microscopic models based on a performance metric. Vehicle count data were collected on simple single-lane networks and used as the benchmark. The chosen metric is the average error, relative to the observations, on the individual values of travel time [18], gaps between vehicles [16], or spacing, speed, and acceleration [21]. The set of parameters of the different models is, at the same time, calibrated on the data, and the selected set is the one that optimizes the chosen metric. Such a statistical method for calibration has been used in many comparative micro-simulation tools studies for more complex and realistic cases, but not for benchmark purposes [15, 22–24]. To our knowledge, no generic methodology for benchmarking micro-simulation tools has been developed to assess global traffic behavior. For benchmarks based on empirical data, we can explain this by the following reason. To perform them, it is necessary to make sure that these data describe, in quantity and quality, the whole set of traffic conditions allowing to assess the comparison criterion [25, 26]. Moreover, such data are difficult to collect when the considered networks are simple or when the ground study is not of correct sizing. Thus, instead of empirical data, the use of validated analytical formulations based on the kinematic wave (KW) theory [27, 28], which has shown its relevance in traffic modeling, might be practical.

Also, global traffic behavior must be assessed on a macroscopic scale. Indeed, even if microsimulation software is used to reproduce the individual behavior of vehicles, those tools combine various sub-models, e.g. the car-following (CF) or lane change (LC) ones. Thus, globally assessing the simulation tools' results means considering their sub-models operations and interactions [29]. This global operation is checked at the macroscopic scale, which matches the traffic flow scale. The variables related to this scale are the flow, the density and the flow speed. From those variables, it is possible to assess the capacity drop prediction ability and, for the merges, how the supply is shared, which help to analyze the operation of simulation tools.

The objective of the paper is twofold:

- first, we propose a methodology to assess traffic microsimulation tools' validity in correctly predicting global traffic behavior in the bottleneck sections of urban highways. More precisely, we focus on point-based diverges, i.e. one lane leading to two different lanes), and on extended merges, i.e. two different lanes leading to a two-lane edge reduced downstream to one lane. This methodology consists in comparing the microsimulation tools' results with recognized analytical formulations,
- second, this methodology is applied to three existing tools. Two open-source ones, SymuVia and SUMO, and one commercial, Aimsun, are chosen for a market-representative pool. For the sake of conciseness, no more tools are considered.

Figure 1 provides a graphical conceptual summary of the approach taken in this article.

The paper is divided as follows. Section 2 presents the three chosen simulation tools and their configuration for common test cases. Section 3 deals with a description of merge and diverge operations and a presentation of the chosen related analytical formulations. In Sect. 4, the indicators produced by all simulation tools are compared with the analytical formulations. Finally, Sect. 5 presents a conclusion and a discussion.

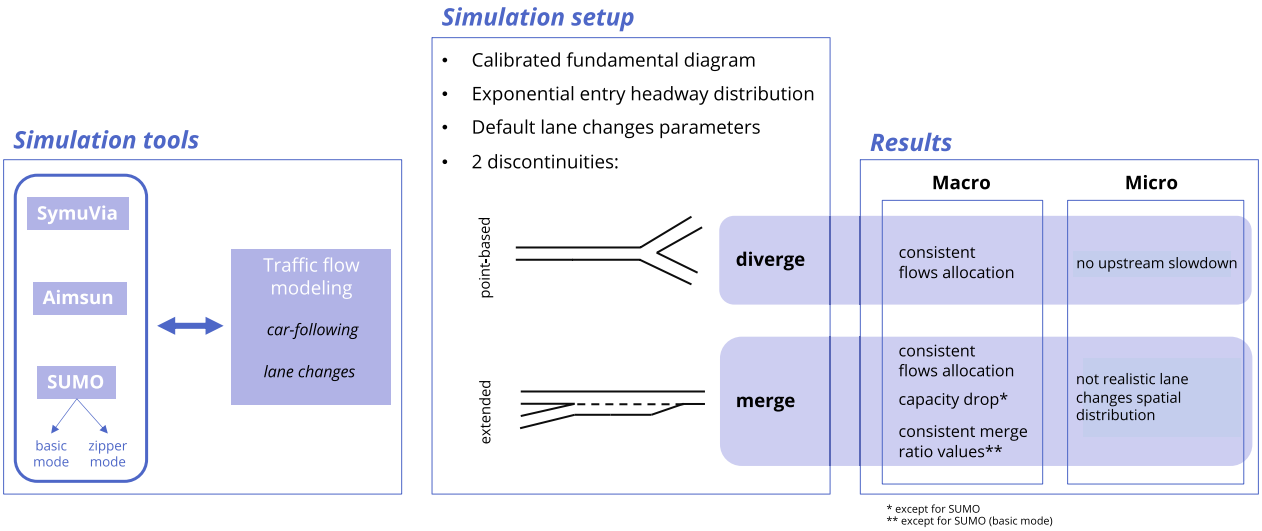


**Fig. 1** Methodology and contribution of the paper

## 2 Presentation and operation of microscopic simulation tools

### 2.1 How microscopic simulation tools reproduce traffic flow situations

In practical terms, microscopic simulation tools reproduce how vehicles move along a network through the numerical discretization of traffic flow models. To do so, they rely on the modeling of the two components of this phenomenon [3]: (i) the assignment model, describing how vehicles are distributed over the different paths of the network, and (ii) the traffic flow model, describing how vehicles progress in the network.

The assignment component relies on an origin–destination matrix summarizing the number of vehicles going from one specific entry zone to one specific exit zone for a given time period [30]. This component will not be detailed further as the users' assignment in the highway discontinuities dealt with here is the simplest possible.

The traffic flow component reproduces the driving behavior of each network user, i.e. at a microscopic scale. These microscopic behaviors are studied under the lens of CF models, LC models, and drivers' heterogeneity, three components explicitly implemented in every simulation tool.

#### *2.1.1 Car-following models*

CF models determine how vehicles longitudinally follow one another on a roadway. This behavior depends on the traffic situation: in free flow, they adopt their desired speed, whereas, in congestion, they maintain a safe distance from their leader, acting on their acceleration. As these models focus on a driver's reaction to the in-front vehicle's actions, various criteria can group CF models into a family of models [31, 32].

An intuitive approach is to characterize the driving psycho-physically. To do so, human factors CF models consider such factors as socio-economic characteristics, aggressiveness, driving style sensitivity, or field of vision, which are directly related to the driver [33]. Some of these models are based on different perceptual thresholds for triggering acceleration, or deceleration [34, 35]. Others are visual angle based and rely on the fact that humans estimate angular changes better than longitudinal distances [36, 37]. Finally, models consider imperfection of the driving, especially the physiological state of the driver, e.g. fatigue and distraction [38, 39].

Taking all human factors into account can be demanding and laborious. Thus, another family of models considers the analysis of human behavior captured in the vehicle's kinematic equations. They are called phenomenological models. Among them, one can mention the first-developed response-stimulus models [40, 41]. They tend to describe the resulting acceleration of the following vehicle as a response to the stimulus, which is the relative speed change. Models in which each vehicle seeks to reach its desired speed while maintaining a large enough gap with the in-front vehicle, to avoid a crash if this one suddenly brakes are safety distance—or collision avoidance—ones [42, 43]. Finally, other models aim to adapt the following vehicle's speed depending on its spatial headway and relative speed; they are called optimal velocity models [44, 45].

However, it is usually not trivial to establish the macroscopic formulation of a CF model that is based on human factors or that is phenomenological. This makes

it difficult to understand the consequences of behavioral parameters on the traffic flow. For this reason, Newell [46] proposed an original CF model with a macroscopic law that explicitly solves the Lagrangian KW model with a triangular fundamental diagram (FD).

When presenting the simulation tools in Sect. 2.2, we will focus on the CF models thereof.

#### *2.1.2 Lane change models*

Vehicles' lateral interactions can be distinguished between discretionary LCs and mandatory LCs [47, 48]. Discretionary LCs occur when a driver considers that traffic conditions on the target lane are more beneficial than the ones on its current lane, e.g. when a truck is in front of the vehicle. Such "comfort" considerations differ from one driver to another, making the LC choice triggering complex to model. After that, the driver checks if the LC can be achieved in complete safety.

Mandatory LCs occur when drivers must change direction to reach their destination, e.g. near highway discontinuities. Some models are based on the game theory, where the decision-making process is mainly based on the collision risk, and very few others on discrete choices. However, most of the existing models are based on the acceptance gap theory [3, 49, 50]. It states that if the inserting-in offered gap is larger than a driver's specific threshold, i.e. large enough to ensure a safe maneuver, then the maneuver is carried out.

Such processes, discretionary and mandatory LCs, are partly based on various parameter thresholds that differ from user to user. It is thus complex to model. The simple diverge and merge operations dealt with in this article induce mandatory LCs only. Thus, mandatory LCs modeling only will be detailed when presenting the simulation tools' models.

#### *2.1.3 Drivers' and vehicles' heterogeneity*

Drivers' and vehicles' heterogeneity deals with how traffic parameters used for the modeling may vary from one driver-vehicle couple to another. This variability applies all the more to the microscopic scale because drivers' behaviors and vehicles' characteristics are different [51]. Since traffic flow comes from the sum of individual behaviors, the induced stochasticity may result in significantly different macroscopic traffic states from the expected ones. It might explain phenomena such as capacity drop, traffic hysteresis, or stop-and-go waves [52–54]. Also, when it comes to simulation software, implemented CF and LC models intend to incorporate this heterogeneity. It is worth noting that along with numerical errors and randomness, the way those models process microscopic parameters is a source of uncertainty. Thus, simulated outputs remain uncertain too [29].

### 2.2 Presentation of the three microscopic simulation tools

The simulation tools are presented together with their default CF and LC implemented models and default insertions and desertions computation. The building of a single reference state, to compare their results on a common basis, is also presented.

#### *2.2.1 The need for a shared macroscopic basis*

As three simulation software are compared, they need to be used on a common basis, i.e. parameters related to the CF models only are calibrated, and the other ones keep their default value. Variability for those critical parameters is not considered, as the analytical models used for the benchmark do not explicitly account for it; see part 3. This calibration of microscopic parameters is carried out to approach the macroscopic values of Table 1 for each simulation tool, ensuring traffic flows similarly between the three tools.

Three parameters common to all the tools are of interest: the desired speed $u$, the minimum spatial gap $g$, and the minimum relative[1] headway $\tau$. Note that in Aimsun and SUMO, the models decompose $g$ into two terms, the vehicle length $l$ and the relative minimum gap $g_{\min}$, so that $g = l + g_{\min}$. Table 2 presents the parameters implemented in the simulation tools. According to the logic of sharing the same macroscopic basis, they were derived from Newell's CF model, which is a macroscopic law one: thus, $u = U$, $g = 1/K$ and $\tau = 1/KW$.

To assess the macroscopic behavior, the FD is checked for each simulation tool, as presented in Fig. 2. In the three cases, the simulated FDs coincide with a triangular one [55] matching with Table 1's parameters, of equation $k \longmapsto \min(Uk\ ;\ W(K-k))$. Thus, the calibration does not need to be expanded further.

#### *2.2.2 SymuVia*

SymuVia is a French open-source simulation tool being developed since 2005 by the Laboratoire d'Ingénierie Circulation et Transports—Éco-gestion des Systèmes Énergétiques pour les Transports [56]. The implemented CF model is adapted from Newell's model [46]. Authors of [57] improved this model by taking into account bounded accelerations, relaxing the original assumption of infinite acceleration ability, and by introducing the relaxation effect with the parameter $\varepsilon$. This parameter is the speed difference of a driver upstream of an inserting vehicle that accepts a smaller insertion

[1] "Relative" refers to bumper-to-trunk values.

**Table 1** Macroscopic expected parameters

| Parameter | Notation | Value |
|---|---|---|
| Free flow speed | $U$ | 70 km/h |
| Backward wave speed | $W$ | 19.4 km/h |
| Jam density (one lane) | $K$ | 150 veh/km |
| Capacity (one lane) | $q_x$ | 2282 veh/h |

**Table 2** Microscopic parameters modified in the simulation tools

| Parameter | Notation | Value |
|---|---|---|
| Desired speed (of vehicle $i$) | $u$ ($u_i$) | 70 km/h |
| Vehicle length (of vehicle $i$) | $l$ ($l_i$) | 5 m |
| Minimum relative gap | $g_{\min}$ | 1.67 m |
| Minimum relative headway | $\tau$ | 1.23 s |
| Maximum acceleration (of vehicle $i$) | $a$ ($a_i$) | 3 m/s$^2$ |

gap than the equilibrium one. This difference applies until the equilibrium gap is reached. The position of vehicle $i$, preceded by leader vehicle $i-1$, at time $t+\Delta t$ is expressed as:

$$x_i(t+\Delta t) = \min\left(x_i^{\mathrm{FF}}(t+\Delta t);\ x_i^{\mathrm{C}}(t+\Delta t)\right) \quad (1)$$

with the free-flow component:

$$x_i^{\mathrm{FF}}(t+\Delta t) = x_i(t) + \min\left(u_i\ ;\ v_i(t)+a\Delta t\right)\Delta t$$

and the congestion component:

$$x_i^{\mathrm{C}}(t+\Delta t) = x_{i-1}(t) + v_{i-1}(t+\Delta t)\Delta t - \frac{\Delta N_i(t+\Delta t)}{K(v_{i-1}(t+\Delta t))}$$

where $\Delta N_i(t+\Delta t)$ is the difference of cumulative vehicles between vehicles $i-1$ and $i$ at time $t+\Delta t$: $\Delta N_i(t+\Delta t) = \min(1;\ \Upsilon \times \Delta N_i(t))$, with $\Upsilon = (1/K(v_{i-1}(t) + v_{i-1}(t+\Delta t) - v_{i-1}(t)+\varepsilon)\Delta t)K(v_{i-1}(t+\Delta t))$. $K(v)$ is the congestion density associated to speed $v$: assuming a triangular FD, $K(v) := \dfrac{1}{g+v\tau}$.

The LC model is an adaptation of [58], described in [57]. It is an extension to the KW model, to the extent that each lane obeys a conservation equation including a creation/desertion flow term related to vehicles changing lanes. The mandatory LCs decisions are probabilistically implemented in the model with, in the creation/desertion flow term, a fraction of vehicles having to change lanes per unit of time equaling the inverse of the simulation time step value. The change is then carried out depending on the capacity of the receiving lane. Relying on the moving bottleneck theory, and in relation with Newell's CF model described above, this model also avoids the over-reaction effect, i.e. the fact that inserting vehicles make their following vehicle instantly stop, in the target lane, due to a spatial gap shorter than the equilibrium one.

#### *2.2.3 Aimsun*

Advanced Interactive Microscopic simulation tool for Urban and Non-Urban Networks is a Spanish commercial simulation tool being developed since 1986, now part of Yunex Traffic, owned by Atlantia [59]. Barceló and Casas [60] describes the implemented CF model. It is an adaptation of Gipps' one [43], which is a safety distance model. This safety distance is derived from ballistic mechanics laws, assuming vehicles have a constant deceleration, as the distance covered by a vehicle if its leader suddenly stops. This derivation leads to calculating a safe speed that operates congested phases.

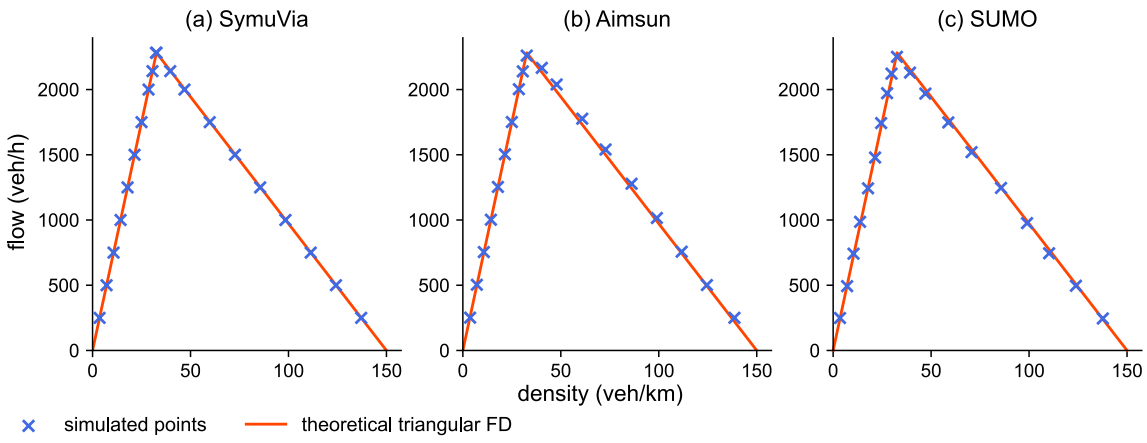


**Fig. 2** Comparison between the simulated fundamental diagrams and a triangular theoretical one

The speed of vehicle $i$ at time $t + \Delta t$ is expressed as:

$$v_i(t+\Delta t) = \min\left(v_i^{\mathrm{FF}}(t+\Delta t);\ v_i^{\mathrm{C}}(t+\Delta t)\right) \quad (2)$$

with the free-flow component:

$$v_i^{\mathrm{FF}}(t+\Delta t) = 2.5 a_i \Delta t\left(1-\frac{v_i(t)}{u_i}\right)\sqrt{0.025+\frac{v_i(t)}{u_i}}$$

and the congestion component:

$$v_i^{\mathrm{C}}(t+\Delta t) = \left((b_i\Delta t)^2 + b_i[2(x_{i-1}(t)-l_i-x_i(t)) - v_i(t)\Delta t + \frac{v_{i-1}(t)^2}{b'_{i-1}}]\right)^{1/2} - b_i\Delta t$$

where:

- $b_i$ is the maximum deceleration of vehicle $i$, in absolute value,
- $b'_{i-1}$ is the estimated maximum deceleration of the leader, in absolute value,

Then, position of vehicle $i$ is derived as $x_i(t+\Delta t) = x_i(t) + v_i(t+\Delta t)\Delta t$.

The implemented LC model is an improvement of Gipps' one [61], described in [60]. Concerning mandatory LCs, the model is based on the gap acceptance theory. It divides the section upstream of the LCs positions into three zones, mandatory LCs modeling mainly acting on the downstream one. In this zone, LCs are carried on only if the braking of the upstream vehicle in the new lane, induced by the inserting vehicle, is safe enough. By the logic of Gipps' CF model, this occurs if the braking distance and a safety margin specific to the inserting vehicle allow for avoiding a collision with the follower. The main difference with Gipps' original LC model is that in the downstream zone, drivers having to change lanes that already waited for more than a threshold time can get impatient and thus reduce their safety margin. The model was also adapted in Aimsun to include courtesy behavior: in the case of on-ramp merges, a fixed proportion of vehicles in the target lane adapt their driving to offer a large enough safe gap to a vehicle willing to insert.

#### *2.2.4 SUMO*

Simulation of Urban MObility is a German open-source simulation tool being developed since 2001 by the German Aerospace Center [62]. Various CF models are implemented in the simulation tool, but the default and most used one is adapted from Krauß' [63]. This is a safe distance model, the main difference with Gipps' being the integration of drivers' imperfection in congested phases, making the speed lesser than expected. Following [64], the speed of vehicle $i$ at time $t + \Delta t$ is expressed as:

$$v_i(t+\Delta t) = \tilde{v} - r\sigma\min\left(\tilde{v};\ a\Delta t\right) \quad (3)$$

Here, $\tilde{v} := \min\left(v_i^{\mathrm{FF}}(t+\Delta t)\ ;\ v_i^{\mathrm{C}}(t+\Delta t)\right)$, with the free-flow component:

$$v_i^{\mathrm{FF}}(t+\Delta t) = \min(v_i(t) + a\Delta t\ ;\ u_i)$$

and the congestion component:

$$v_i^{\mathrm{C}}(t+\Delta t) = v_{i-1}(t) + \frac{x_{i-1}(t) - l_i - x_i(t) - v_{i-1}(t)\tau}{\frac{v_{i-1}(t)+v_i(t)}{2b} + \tau}$$

where:

- $b$ is the maximum deceleration, in absolute value,
- $\sigma$ is a fixed value in [0; 1] capturing the drivers imperfection, together with the random value $r$ uniformly distributed in [0; 1]. Note that if equation 3 returns a negative value due to the distribution of $r$, a null value is returned when updating $v_i$. Under the assumptions of 2.2.1, $\sigma$ is set to 0 in our simulations.

As for Gipps' model, position of vehicle $i$ is then derived as $x_i(t+\Delta t) = x_i(t) + v_i(t+\Delta t)\Delta t$.

The implemented LC model is described in [65]. Just as in Gipps' LC model, the mandatory LC of an inserting vehicle is carried out only if the gap chosen by this vehicle is large enough to induce that the speed of the upstream vehicle on the new lane is safe enough to prevent a collision. This mandatory LC is triggered depending on its urgency, based on the target lane's density, the distance before the obstacle in the route, and the vehicle's speed when approaching this obstacle. Suppose the LC cannot be carried out; the model checks if the inserting vehicle's speed has to be adjusted because blocked by its leader in its departure lane. Next, the model checks if the speed of the upstream vehicle on the new lane has to be adjusted to offer a large enough gap to the inserting vehicle.

It is also important to note that concerning operating merges, SUMO provides an explicit easy-to-configure mode aiming to reproduce the zipper effect of the Newell–Daganzo operation model (see part 3.2), which will also be dealt with in our cross-comparison. As a consequence, we will present, for SUMO, the merge results when this mode is active, referred to as the zipper mode, and when it is not, referred to as the basic mode.

**Table 3** Notations used for the diverges and merges modeling

| Definition | Notation |
|---|---|
| Proportion of diverging vehicles | $\beta$ |
| Downstream bottleneck capacity on lane $i$ | $C_i$ |
| Merge/priority ratio | $\alpha$ |
| Demand (demand on lane $i$) | $\lambda$ ($\lambda_i$) |
| Effective flow (effective flow on lane $i$) | $q$ ($q_i$) |

## 3 Analytical modeling of traffic discontinuities

After presenting how simulation tools process insertions and desertions, the analytical modeling of their resulting macroscopic effects is examined. Table 3 sums up the notations of the models.

### 3.1 Point-based diverges analytical behavior

A predetermined two-lane choice between exit 1 and exit 2 of potentially different capacities—see Fig. 3a—is offered to drivers, $\beta$% of them choosing lane 1. As there are two downstream lanes and only one upstream, it is crucial to set up traffic conditions that induce congestion. Indeed, if one of the lanes is congested, congestion goes backward until the upstream lane. To determine the effective flows in such a case, Newell [66] suggested the *first in, first out* (FIFO) rule. It stipulates that the vehicles' order of appearance at the diverging point is the same as the one upstream of this point or that the travel times upstream of the diverging point are the same, whatever the destination is.

A graphical tool describing traffic operation for a diverge that integrates the FIFO rule, referred to as the diverge diagram, is presented in [67] and exposed in Fig. 3a:

- the free-flowing operation corresponds to zone 1 and is observed when the demand $\lambda$ does not exceed the minimum capacity of the three lanes. Then, the operation point is $(q_1 = \beta\lambda; q_2 = (1-\beta)\lambda)$,
- else, the congested operation holds:
  - if $\beta$ is too low so that lane 2 is congested, i.e. $\lambda_1{:=}\beta\lambda < C_1$ and $\lambda_2{:=}(1-\beta)\lambda > C_2$, then the operation point is $(q_1 = \frac{1-\beta}{\beta}C_2; q_2 = C_2)$. This is graphically detailed on Fig. 3a,
  - by symmetry, if $\beta$ is too high so that lane 1 is congested, then the operation point is $(q_1 = C_1; q_2 = \frac{\beta}{1-\beta}C_1)$.

Although synthetic, this modeling does not incorporate on-field observed phenomena occurring near the diverge point, like lower speeds [68–70]. These phenomena can induce a capacity drop [70]. To fill this gap, [71] developed an analytical formulation based on the moving bottleneck theory [72, 73], validated with micro-simulations. It captures vehicles' anticipation before changing lanes to get the right path, reflected by lower speeds upstream of the diverging point. This anticipation then induces an in-front void that may cause a capacity drop. In addition to these microscopic considerations, most highway diverges are located on multi-lane highways. Authors of [6, 70] observed empirically that, in this case, the FIFO rule does not stand, as upstream vehicles can change lanes and will not be blocked anymore, impacting the capacity. Finally, note that this point-based diverge setup was also chosen to ensure no discretionary LC is triggered, permitting the comparison of simulation tools on a simple basis.

### 3.2 Extended merges analytical behavior

The general principle of the merge modeling is to distribute the downstream capacity $C^{\mathrm{m}}$ on lanes U and R, according to the demands $\lambda_{\mathrm{U}}$ and $\lambda_{\mathrm{R}}$. One of the most used is the Newell–Daganzo model [74, 75], for its simplicity.

This model is synthesized in Fig. 3b. Given the demands, each lane is allocated effective flows $q_{\mathrm{U}}$ and $q_{\mathrm{R}}$, which may be lower than the demands, as the sum of the demands may exceed the effective capacity of the merge. The allocation is based on a projection of demands on the downstream capacity curve, parameterized by $C^{\mathrm{m}}$. This is shown in Fig. 3b in the simple case where the merge capacity equals $q_x$, *a priori* an exogenous parameter. Lane R inserts on lane U, with a merge ratio $\alpha$. The merge ratio definition also has been discussed, but, on a theoretical basis, some authors claim that this is the ratio of the effective upstream capacities [76]. As those capacities are known to be proportional to the number of lanes, a good approximation of $\alpha$ is the ratio of the number of lanes, as experimentally proven by [77]. Note that this does not hold when downstream traffic conditions impact the merge [78], which is not the case in our framework.

The allocation then depends on the demand on each lane:

- while the sum of the demands does not exceed the merge capacity, each demand is satisfied, and the projection function is null (i.e. the operation point is $(q_{\mathrm{U}} = \lambda_{\mathrm{U}}; q_{\mathrm{R}} = \lambda_{\mathrm{R}})$), which corresponds graphically to zone 1,
- if the sum exceeds the merge capacity, then at least one upstream lane is congested:

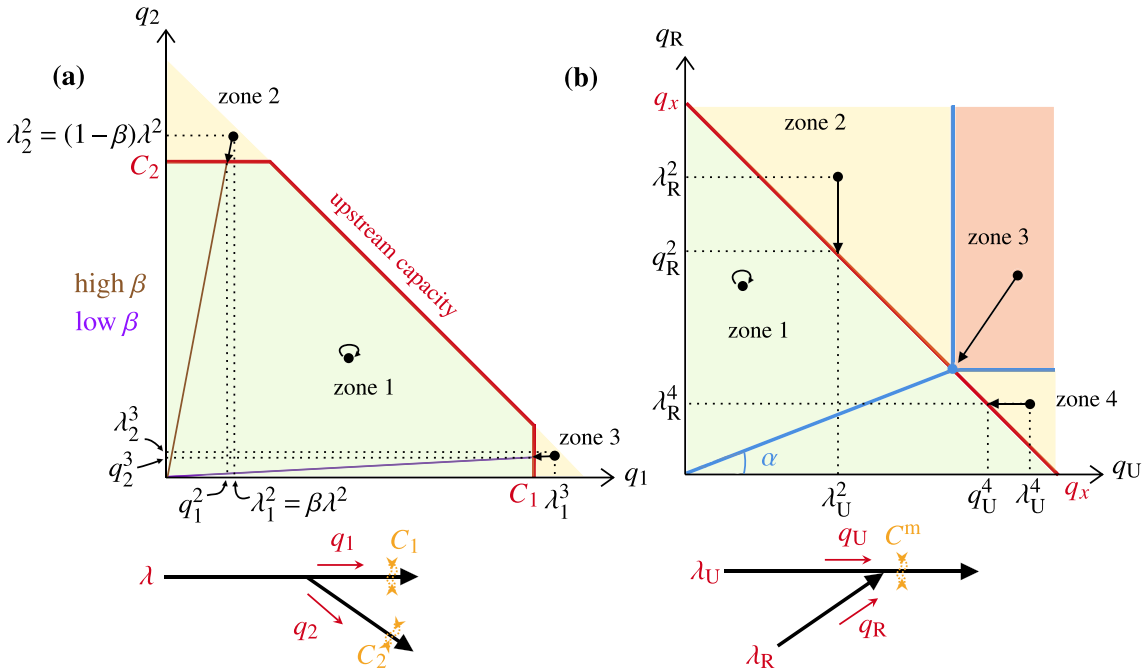


**Fig. 3** Diverge and merge analytic behaviors: **a** diverge diagram [67] with constant downstream and upstream capacities and **b** Newell–Daganzo diagram [74, 75] in the case the downstream capacity is constant ($C^m = q_x$); with their and allocation schemes, and associated notations and networks

- if lane R is congested and if lane U is free-flowing, then the projection function acts on the demand of lane R, which cannot be satisfied, unlike the one of lane U (i.e. the operation point is $(q_U = \lambda_U; q_R = C^m - \lambda_U)$), see zone 2 on Fig. 3b,
- by symmetry, we have, for zone 4, the operation point $(q_U = C^m - \lambda_R; q_R = \lambda_R)$,
- if both lanes are congested, only one operation point is possible, and all demands are projected on it: it is such as $q_R = \alpha q_U$, see zone 3.

This model reflects the fact that when both lanes are congested, vehicles from upstream lanes enter the downstream lane each in turn, the frequency of the giveaway being determined by the merge ratio. This is called the zipper effect [78]. Following Fig. 3b, the higher the $\alpha$, the higher the priority of lane R vehicles.

Although very simple, this model is in adequacy with empirical observations on highway loops [77, 79–81], whether for the priority ratio existence in general congestion or the share of the capacity when only one type of lane is congested.

However, the Newell–Daganzo model does not capture the capacity drop observed at highway merges. Such drops are documented for several decades and can reach more than 20% [8, 82, 83]. The source of the drop has been discussed a lot, as various microscopic phenomena could induce a drop: acceleration after lane change that can create voids; heterogeneity in gap acceptance; length of the merge and distribution of insertions; or different insertion speeds [7, 58, 84]. Authors of [7] developed an analytical formulation of the macroscopic capacity curve based on the variational theory [85]. This modeling extends the Newell–Daganzo model by capturing the microscopic behaviors dealt with beforehand. It was validated with a set of on-field data from sensors of a British highway, providing speeds and flows to identify congested situations that were found to fit the developed analytical model.

## 4 Simulation tools and traffic discontinuities operation: cross-comparison

### 4.1 Methodology

The simulated diverge and merge are shown in Fig. 4. The networks are identical for all simulation tools. Simulated sensors provide, every 15 s, the values of flow, density and speed.

#### *4.1.1 Generating the diverge operation results*

To examine the diverge macroscopic operation, congestion is gradually generated in the network. To do so:

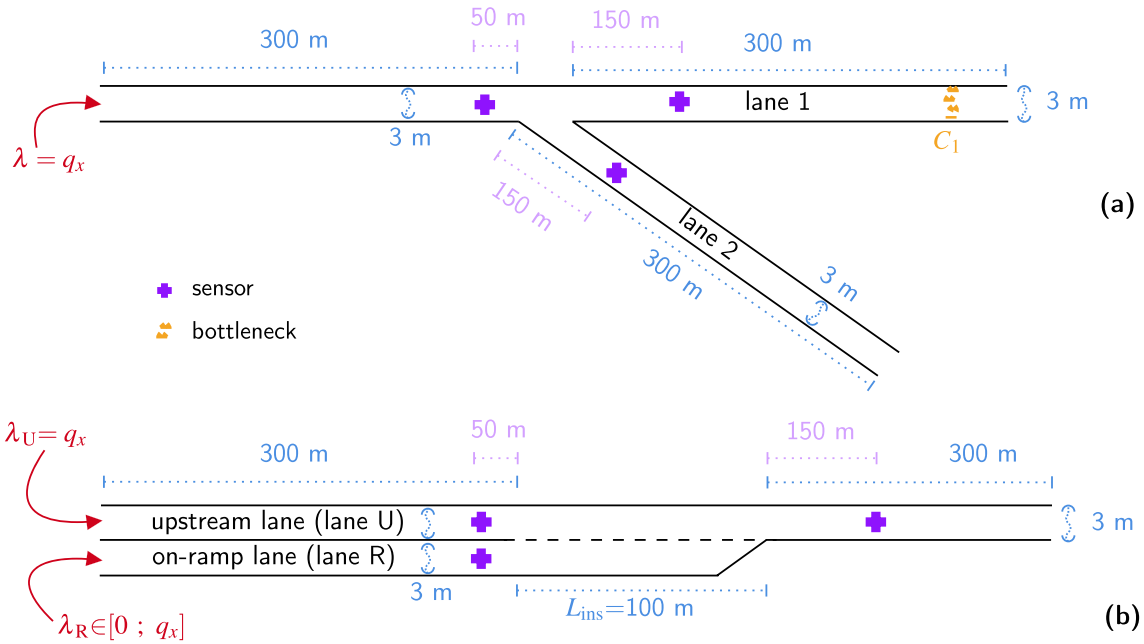


**Fig. 4** Networks used for a diverge with **a** a downstream bottleneck and **b** for an extended merge

- the upstream lane inflows at capacity, but as both downstream lanes capacity is $q_x$, we need to implement, on one lane—lane 1 here—, a bottleneck of capacity $C_1 \leq q_x$ to examine the congested operation of the diverge. Thus, we produce various diverge diagrams by taking 5 values of $C_1$ from 0 veh/h to $q_x$, with a 25% increase from one value to another. To avoid a complete gridlock, instead of 0 veh/h, we arbitrarily chose a value of 3% $q_x$,
- for each value of $C_1$, one step accounts for a value of $\beta$, from 0 to 100% with a 25% increase from one step to the next,
- for each step, 15 replications of one hour of traffic are simulated,
- every selected flow is the mean of the flow during the 15 last minutes.

Note that we did not consider the reverse case where the bottleneck is located on lane 2 because of the problem's symmetry.

#### *4.1.2 Generating the merge operation results*

To examine the extended merge macroscopic operation of simulation tools, i.e. the downstream supply sharing and the capacity drop, congestion is gradually generated on the network. A synthetic way of retrieving such indicators is the Newell–Daganzo diagram. To create it, the following methodology is considered:

- the main lane inflows at capacity,
- the on-ramp lane uniformly increases its inflow from null to capacity by 10 steps (excluding the step in which the inflow is null),
- for each step, 15 replications of one hour of traffic flow are simulated,
- to be sure a potential warm-up phase has elapsed, every selected flow is the mean of the flow during the 15 last minutes.

Note that we did not consider the reverse case where the on-ramp would be inflowing at capacity and the main lane would increase its inflow because of the problem's symmetry.

To illustrate our results, we will also focus on specific configurations. There are three of them:

(a) a free flow case ($\lambda_U = \lambda_R = 500$ veh/h), referred to as FF/FF,
(b) a case where the upstream lane only is congested ($\lambda_U = q_x$ and $\lambda_R = 0.3q_x$), referred to as CC/FF,
(c) and a case where the upstream and on-ramp lanes are congested ($\lambda_U = \lambda_R = q_x$), referred to as CC/CC.

### 4.2 Entrance time headways distribution

Before investigating macroscopic behaviors of simulation tools, we find it relevant to compare the way they

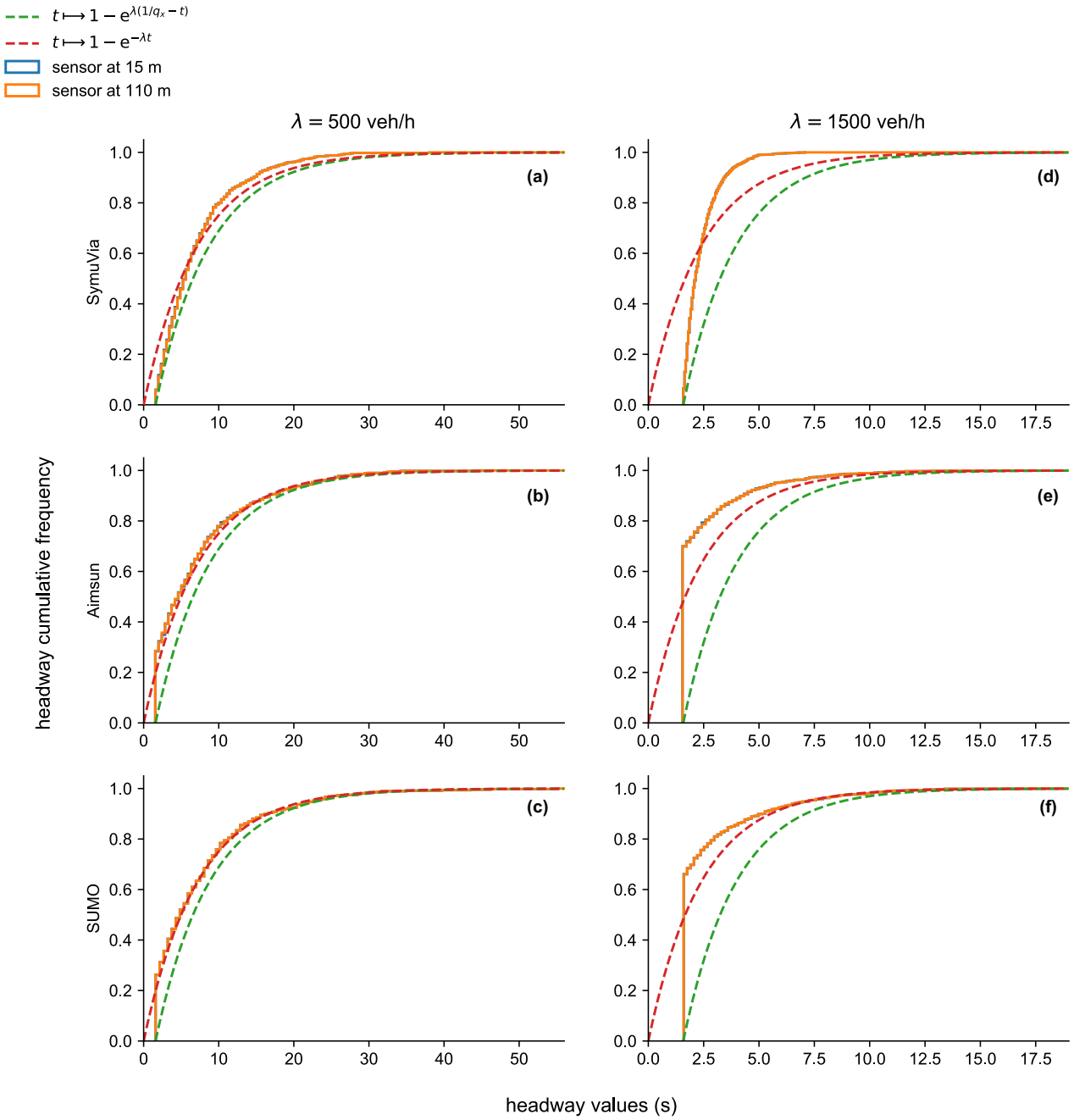


**Fig. 5** Vehicles generation: comparison of the entry headways distribution with a theoretical exponential distribution for a demand of **a**–**c** 500 veh/h and of **d**–**f** 1500 veh/h

generate vehicles at the entrance of a network, as the time headways distribution may contribute to a capacity drop near highway discontinuities [7, 71].

Among the different distributions that can be implemented for entrance time headways, the exponential one fits best with on-field observations [86, 87]. More precisely, the time entrances of vehicles follow a Poisson process so that the headways follow an exponential distribution. We then configured the simulation tools so that the distribution of entry headways is exponential, in which the mean equals the inverse of the demand. Note that SUMO explicitly generates vehicles following a Bernoulli process, which asymptotically converges to a Poisson process.

The way vehicles are generated in a free-flow situation is now deeper investigated. Figure 5 presents the cumulative distribution of simulated net headways for two free flow demands and two sensors 95 m apart. The first one is located at the entrance of the network. The considered network is a simple lane of capacity $q_x = 2282$ veh/h (see Table 1), where the demand inflows during one hour.

For each simulation tool and both levels of demand, there is no significant difference in the observed distribution. This means that the implementation of CF models in the simulation tools does not induce spatial variability on the headways. No simulated headway is lesser than $1/q_x$, which is a minimum headway. This is consistent with the three CF models implemented, whether Newell's one or collision avoidance ones, as the models consider the leader to be distant from its follower a sufficient distance. Consequently, for a low demand with 500 veh/h, the resulting headways distribution should be a $1/q_x$ -shifted exponential distribution [86]. However, looking at Aimsun and SUMO's cumulative distributions, see Fig. 5b, c, all values of headways less than $1/q_x$ are projected on the value $1/q_x$.

Finally, headways deviate from an exponential distribution for a higher demand of 1500 veh/h and are gathered around the minimum headway. Indeed, as more vehicles are in the network, large headways are scarce [88].

### 4.3 Point-based diverge operation results

Figure 6 presents the diverge diagrams for each simulation tool, according to the methodology of Sect. 4.1.1. As the simulated flows are projected on the grey dotted lines in Fig. 6, the diverging flows are consistent, so the operation is correctly reproduced (result 1.1). However, no significant capacity drop is observed for any simulation tool, as the theoretical shape matches with simulated effective flows for both free-flowing and congested cases (result 1.2). This means that the deceleration assigned to lane changes anticipation [71] is not implemented in the simulation tools for the simple case of a point-based diverge (result 1.3). We however do observe a slowdown of vehicles aiming to diverge in Aimsun, but as highlighted by Fig. 6b, it does not induce a drop.

### 4.4 Extended merge operation results

#### *4.4.1 Macroscopic operation results*

To introduce the macroscopic results, Figs. 7 and 8 present, for each simulation tool, the speed and flow time evolution for the three sensors in the network (see Fig. 4b). They match with traffic cases FF/FF, CC/FF and CC/CC described in 4.1.2. For each simulation tool and traffic case, values are the ones of a single simulation. The curves are smoothed with an aggregation period of 2 min. Note that the same random seed was taken for both SUMO modes to compare them on the same replication. Expected flows are the theoretical ones derived from [7], incorporating capacity drop effects. The speed analysis in Fig. 7 shows that simulation tools reproduce the merge operation correctly. Indeed, when the traffic is free-flowing, the simulated speeds are close to the free-flow speed, while when it is congested, the speed is lower than the free-flow speed. We can notice, in the second row, that speeds on the on-ramp lane exceed the free-flow speed in SymuVia. It may be related to the default operation of this simulation tool when a vehicle coming from the on-ramp lane inserts, overtaking vehicles on the upstream lane.

When it comes to flows, note that in Fig. 8a, b, the flow fluctuations are caused by the departures headways exponential distribution. Also, when the upstream lane only is congested (Fig. 8b), the downstream flow is more or less constant of near-$q_x$ value. It is not the case for Aimsun, the flow being less than $q_x$ on average and fluctuating more. Finally, in all general congestion situations (Fig. 8c) the flows remain more or less constant. No capacity drop is observed for SUMO. SUMO's basic mode operation shows an on-ramp lane flow

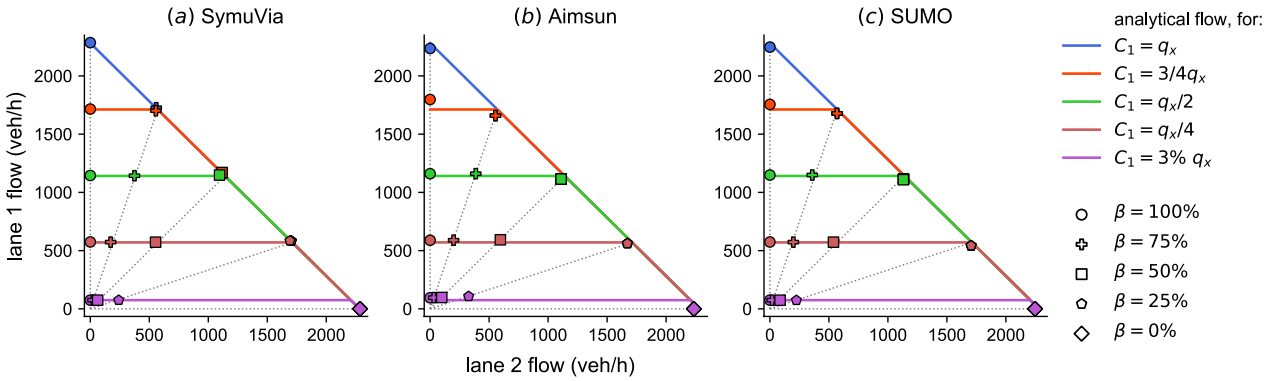


**Fig. 6** Cross-comparison of the simulated diverge diagrams

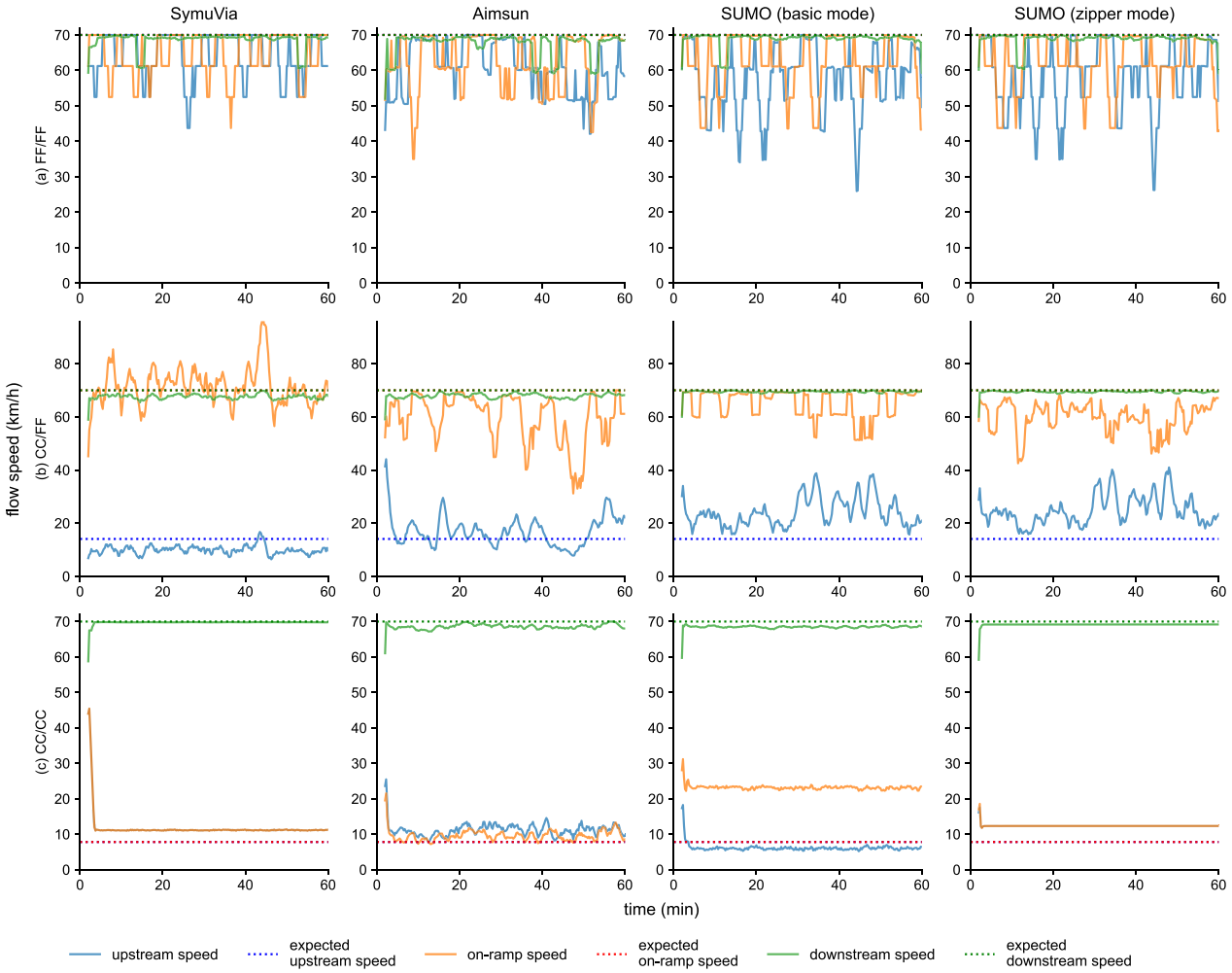


**Fig. 7** Flow-speeds evolution for one simulation, when **a** both lanes free flow; **b** upstream lane is congested and on-ramp lane free flows; **c** both lanes are congested

larger than the upstream lane one, which is not consistent with what is observed on-field [77]. However, flows time evolution is different with Aimsun, which shows fluctuations, although of lesser amplitude and frequency than in a free-flow state. As the capacity drop may be caused by various individual behaviors related to the physics of insertions, and as Aimsun is the only simulation tool capturing a significant capacity drop, it can be considered that such fluctuations are the hallmark of that drop.

Figure 9 provides a more global view with the cumulative flows associated to Fig. 8. Note that a cooldown period is observed after 60 min, so all the demands are null. This first allows to verify that the simulation tools inflow all the demanding vehicles, storing the ones that cannot enter due to congestion just upstream of the network's entry. Second, in the congested cases, the cumulative flow counts are bounded between a curve where the capacity drop is not considered and a curve where it is, derived from the model of [7]. In light of these boundings, the macroscopic behavior of the simulation tools looks consistent, with Aimsun showing a higher capacity drop in congested cases (rows 2 and 3). However, when both lanes are congested (row 3), SUMO's basic mode shows higher cumulative vehicle counts on the on-ramp lane than when there is no drop.

To have a more detailed and precise analysis of these phenomena and to quantify them correctly, Fig. 10

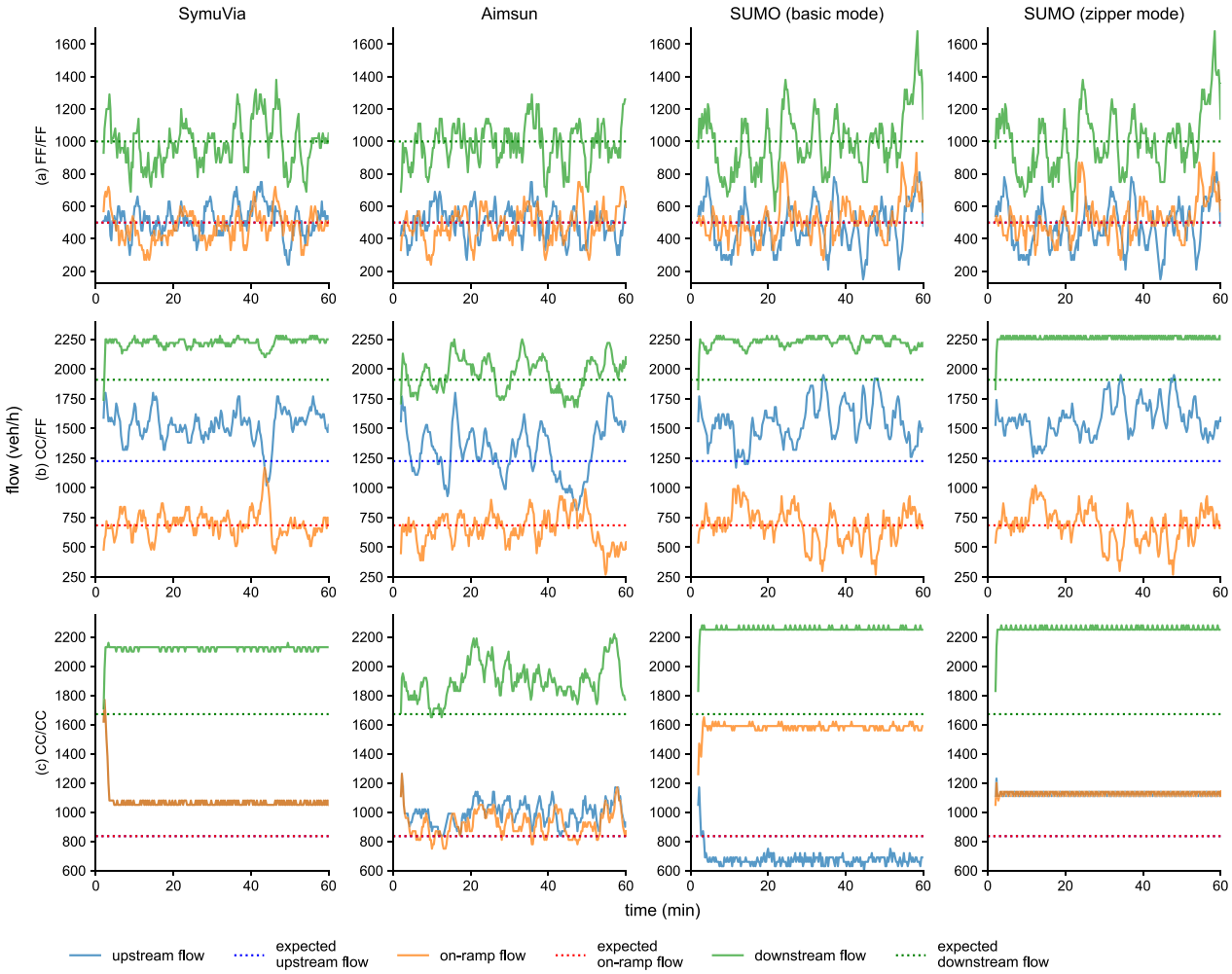


**Fig. 8** Flows evolution for one simulation, when **a** both lanes free flow; **b** upstream lane is congested and on-ramp lane free flows; **c** both lanes are congested

presents the Newell–Daganzo diagrams for each simulation tool, according to the methodology of Sect. 4.1.2. From these diagrams comes Table 4, giving the measured capacity drop in general congestion and the merge ratio. We can notice that the four simulation tools configurations (SymuVia, Aimsun, SUMO's basic mode, and SUMO's zipper mode) can be grouped into two families of merge behaviors. Both respect the fact that the demand is projected on the capacity curve due to the downstream supply restriction. Thus, the macroscopic operation of merges is correctly implemented in every simulation tool (result 2.1).

- The first family of behaviors gathers SUMO's results; see Fig. 10a, b. It is characterized by the absence of significant capacity drop when congestion appears, as the downstream theoretical capacity is shared between the upstream lane and the on-ramp lane. This operation coincides with the theoretical zipper model. In the zipper mode case, the share of the downstream capacity is fair, as the merge ratio equals 1, which is the ratio of the number of lanes of the main way (one) and the one of the on-ramp way (one), what is consistent with on-field data [77]. However, as perceived in Fig. 9, in the basic mode case, the merge ratio is larger than 2. This means that more than two-thirds of the vehicles come from the on-ramp lane. Such a value is too high and unrealistic, as priority is therefore not given to the upstream lane vehicles (result 2.2).
- The second family of behaviors matches with SymuVia and Aimsun's results; see Fig. 10c, d. In this case, the capacity drop is observed (result 2.3), even if lesser than the one predicted by [7]'s analytical model when both lanes are congested. It is worth noting that for SymuVia, the drop appears for higher values

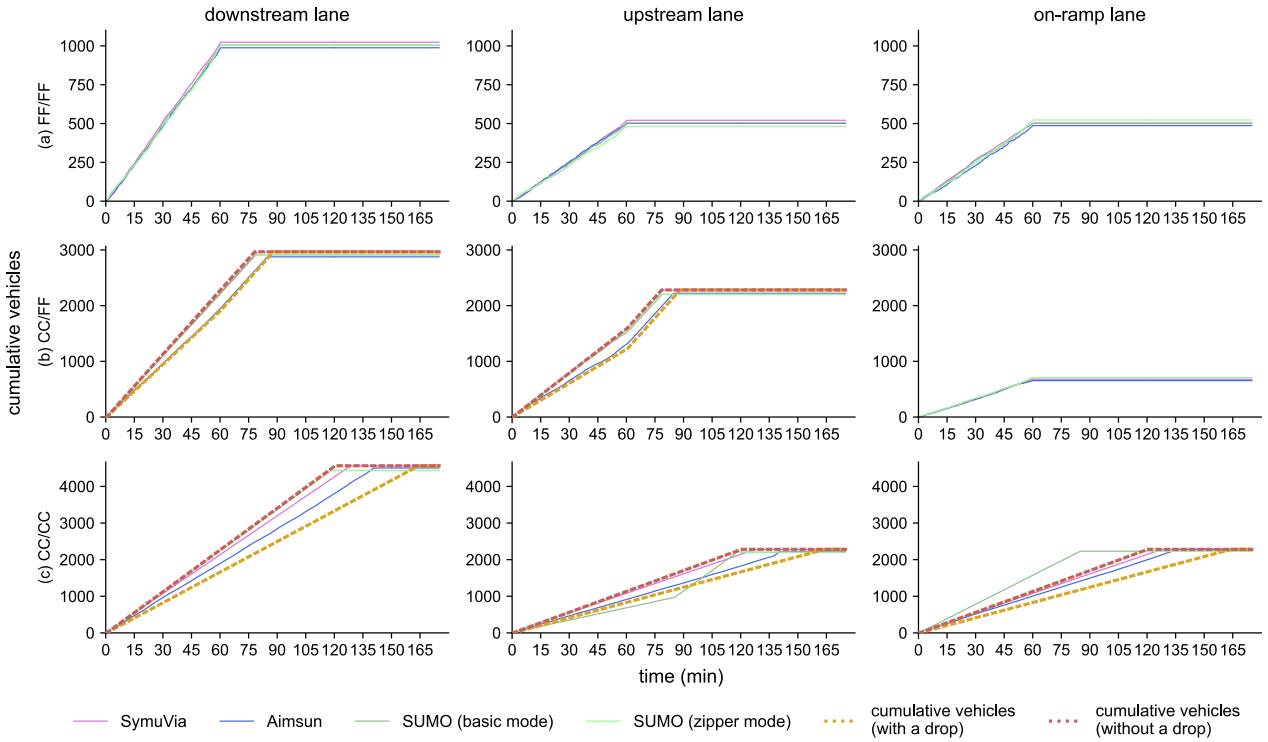


**Fig. 9** Cumulative flows associated to Fig. 8, when **a** both lanes free flow; **b** upstream lane is congested and on-ramp lane free flows; **c** both lanes are congested

of demands. Lastly, the merge ratio is about 1, which is a consistent value as it matches the ratio of the number of lanes [77].

#### *4.4.2 Lane changes positions distribution*

Finally, for the merges, the spatial distribution of LCs is analyzed. Indeed, the variability of this microscopic behavior can have consequences on the congestion's dynamic [7]. Still, with the objective of benchmarking the micro-simulation tools, the parameters of the LCs models implemented in each simulation tool are the default ones.

To introduce this analysis, Fig. 11 shows the vehicles' trajectories on the LCs area of the network of Fig. 4b. Two simulations are considered. They correspond to cases CC/FF and CC/CC. First, we observe that vehicles insert in the last 20 ms for SymuVia and both SUMO's modes, while insertions are more distributed on Aimsun. Second, congestion occurs where on-ramp lane vehicles insert. This is demonstrated by the slowing down of vehicles coming from the upstream lane and the propagation of shock waves induced by these insertions.

To go further, the variability in LCs positions is investigated by representing their distribution; see Fig. 12. As the insertion process differs whether congestion is significant or not [47, 89], the three cases FF/FF, CC/FF, and CC/CC were considered. The simulation times were adapted so that for each simulation tool and each traffic situation, approximately 1500 insertions make up one distribution. Also, note that the shape of the distribution does not change with the size of the insertion edge. Thus we only give and detail the results of the baseline case with a length of 100 ms.

Every LC in SymuVia is located in the last 20 ms of the insertion zone, the LCs getting closer to the end of the zone when the congestion gets severe on the on-ramp lane. Aimsun's results show that LCs are distributed all over the insertion zone, even if closer to the entrance in a free-flowing operation. However, it should be noted that in congestion, many vehicles change lanes at the end of the zone. A possible explanation is that drivers could not encounter any large enough gap before. In SUMO's basic mode, LCs are closer to the beginning of the zone in free-flowing conditions and more distributed in congestion. Finally, SUMO's zipper mode results are the opposite of SymuVia's, as LCs

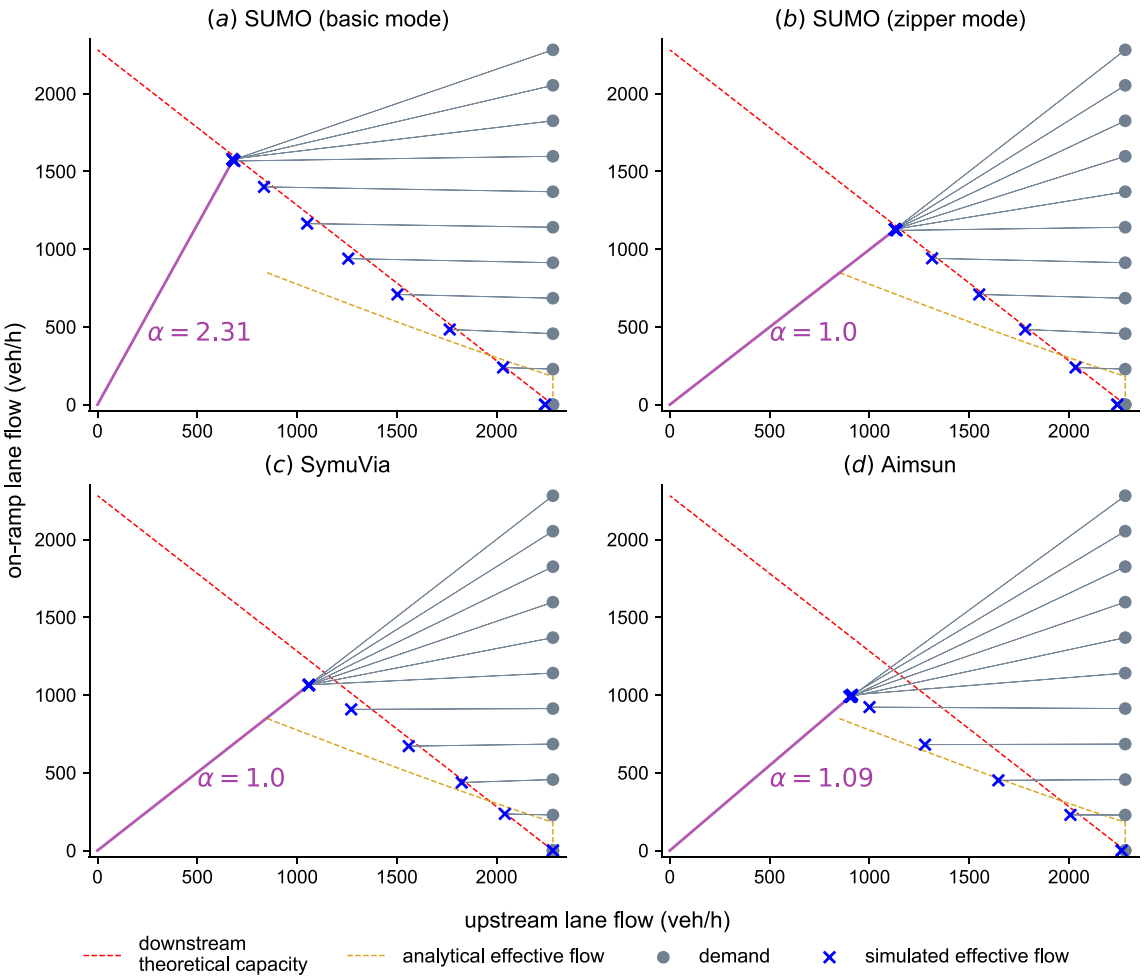


**Fig. 10** Cross-comparison of the Newell–Daganzo diagram. Grey lines match with Newell–Daganzo's projection function

**Table 4** Main simulated macroscopic outputs for the merge operation

| Simulation tool | Maximum capacity drop (%) | Average capacity drop in general congestion (%) | Merge ratio |
|---|---|---|---|
| SymuVia | 7.04 | 6.97 | 1.00 |
| Aimsun | 17.16 | 16.71 | 1.09 |
| SUMO (basic mode) | 3.78 | 1.24 | 2.31 |
| SUMO (zipper mode) | 1.72 | 1.13 | 1.00 |
| *Analytical modeling from* [7] | 25.57 | 25.57 | 1 |

are concentrated at the end of the zone when traffic conditions get free-flowing. However, on-field data on European highways show that the most congested the on-ramp lane, the less distributed and the closer to the beginning of the insertion section the LCs [15, 47]. Thus, as this is not observed in the simulated results, the chosen simulation tools, with their default operation, do not reproduce LCs accurately (result 2.4). However, these remarks will have to be confirmed by a comparative analysis with on-field data, which we do not have. Indeed, to our knowledge, there is no analytical formula for deriving the spatial distribution of lane changes at merges.

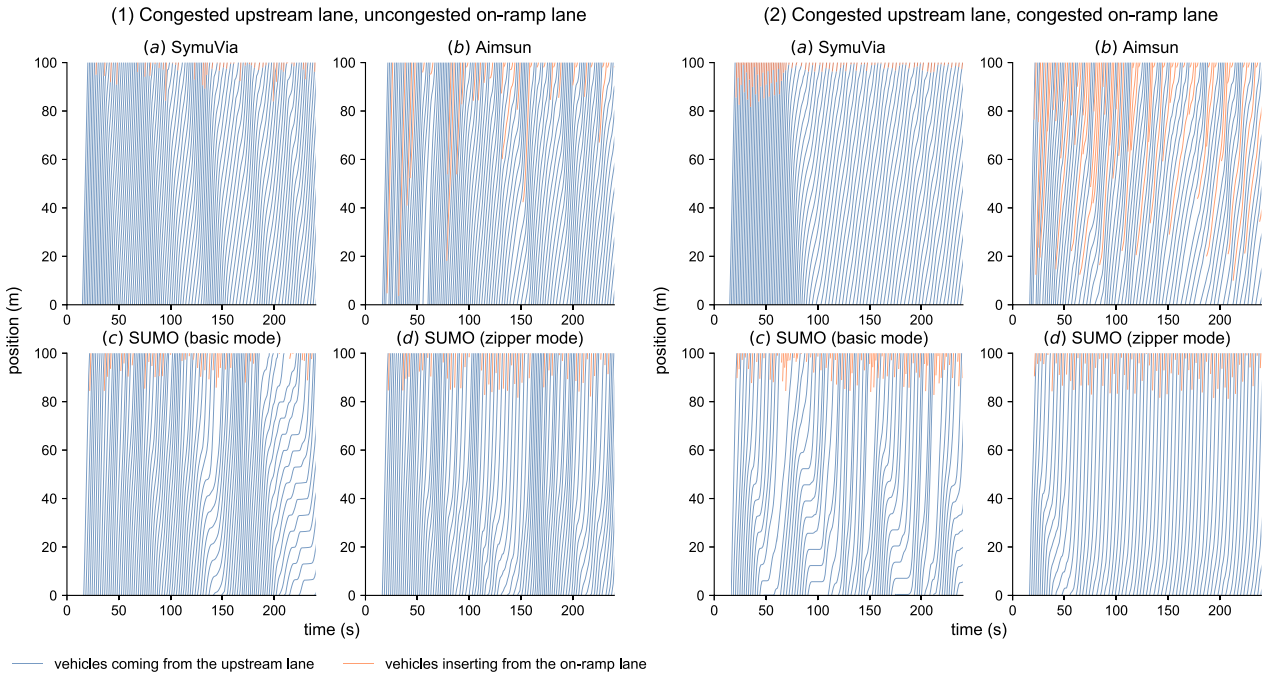


**Fig. 11** Vehicles trajectories on the extended merge LCs zone when (1) the upstream lane is congested and on-ramp lane free flows; and (2) both lanes are congested

## 5 Discussion and conclusion

This investigation aimed to provide a generic benchmark method for traffic microscopic simulation tools capability to reproduce global traffic behavior. We focused on the cases of merges and diverges. Indeed, these two bottleneck configurations permit to cover the traffic phenomena occurring at all the other bottlenecks of urban highways: a weaving section is a merge upstream of a diverge; a lane-drop section is very similar to a merge section.

This generic benchmark method car be synthesized as follows:

- first, to ensure that this comparison was made on the same shared basis, i.e. the FD is roughly the same, we only modify the following microscopic values: the desired speed, the relative headway, and the minimum spatial gap,
- second, we propose a set of simple cases that are reproduced in the simulation tools, a point-based diverge and an extended merge,
- third, we identify the validated analytical formulations defining each test case's expected behavior and compare them to the simulated results.

For the three chosen simulation tools, the main results can be synthesized as follows:

- regarding diverges operation:
  - *result 1.1*: the macroscopic behavior is correctly reproduced,
  - *result 1.2*: no capacity drop could be highlighted,
  - *result 1.3*: upstream of the diverging point, no significant vehicles' slowdown was brought out,
- regarding merges operation:
  - *result 2.1*: the macroscopic behavior is correctly reproduced,
  - *result 2.2*: every configuration presents an equitable sharing of the downstream supply, except SUMO's basic mode, which presents an unrealistic one,
  - *result 2.3*: a capacity drop is identified in SymuVia and Aimsun but not in SUMO. The maximum capacity drop highlighted by Aimsun, around 17%, is higher than the one in SymuVia, around 7%, consistent with on-field observations values, between 5 and 30% [8, 9],
  - *result 2.4*: for every configuration, the behavior of inserting vehicles is not in agreement with experimental observations. It is worth noting that this result needs to be further investigated by a comparative analysis with on-field data.

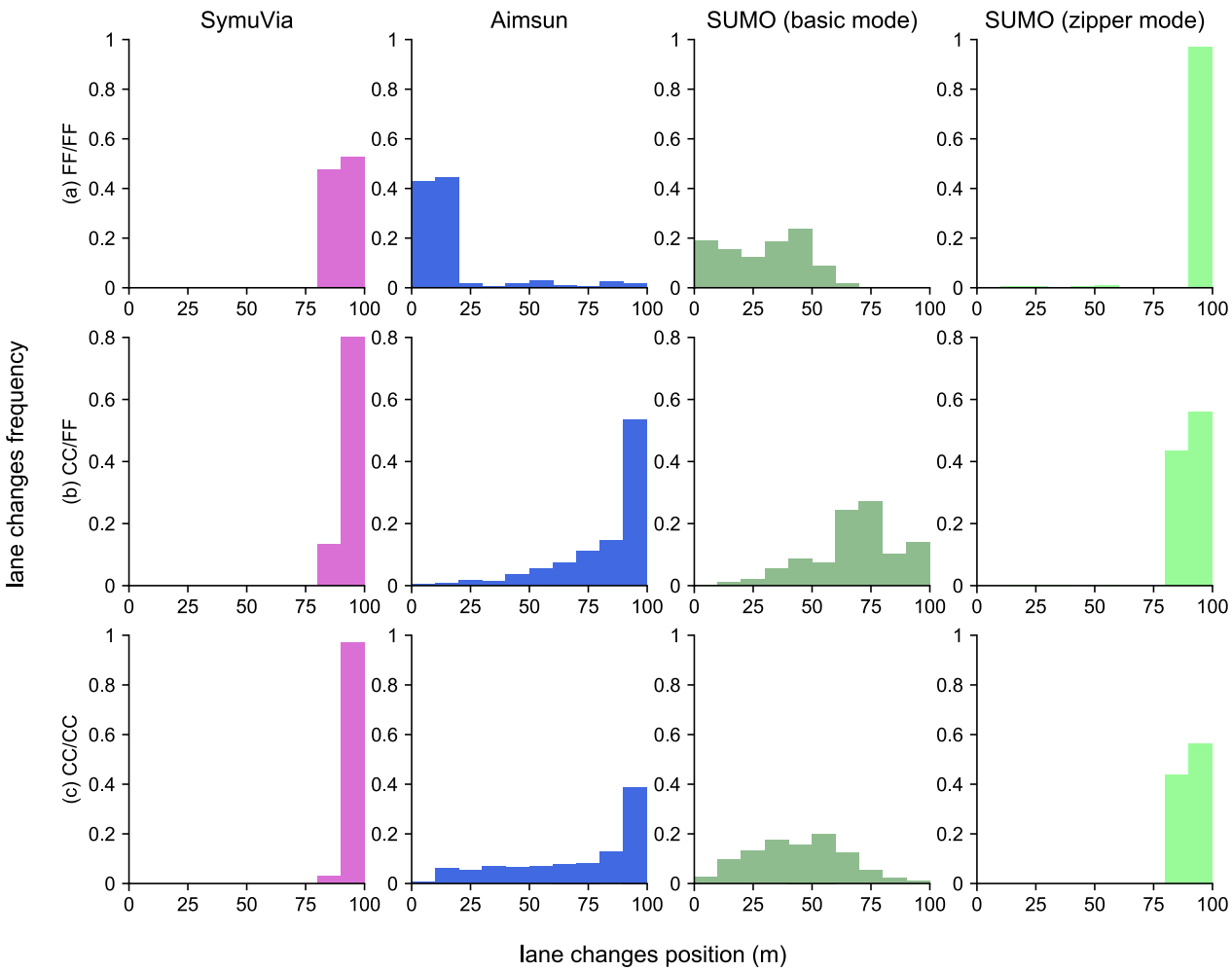


**Fig. 12** Distribution of simulated lane changes positions upstream an extended merge, when **a** both lanes free flow; **b** the upstream lane is congested and on-ramp lane free flows; **c** both lanes are congested

However, as our observations stand for a very simple simulation framework, there are limitations to these results. First, the number of simulation tools to be benchmarked should be increased to have a more accurate insight into the default behavior of most of the simulation tools used by public authorities and design offices. Here, we limited ourselves to three tools to be concise. Second, we focused on straightforward cases of merges and diverges. The framework would benefit from being used for more realistic cases with multiple lanes. This requires either adapted analytical models or sufficient quality field data as the reference for the benchmark. Next, the basic assumption of this benchmark, relying on the fact that few parameters were changed, may explain why no capacity drop was observed at diverges. Thus, to explain this lack of drop, extensive work should focus on the impact of the other parameters in the CF models, such as the deceleration for safety-distance-based models, or in the LC models. Finally, we did not consider the stochasticity of the microscopic parameters used, as it is not taken into account in the chosen analytical formulations. It should be examined in more detail since it can significantly impact traffic indicators values in congestion, such as queue lengths, for sophisticated networks in simulation [90]. After the conclusions of this future work and having modified the simulation tools' default values or the CF and LC models accordingly, looking to those more elaborated networks will begin to be conceivable.

**Abbreviations**

| | |
|---|---|
| HOV | High-occupancy vehicle |
| KW | Kinematic wave |
| FD | Fundamental diagram |
| CF | Car-following |
| LC | Lane change |
| FIFO | First in, first out |

**Acknowledgements**
The authors thank Cécile Bécarie from the LICIT- Éco7 lab for her precious assistance when using the SymuVia platform, as well as Tamara Djukic from Aimsun SLU.

**Author contributions**
ChB and NC coordinated the study and validated the methodology. MB prepared and ran the simulations, cleaned the output data, analyzed the results and designed the figures. ChB and MB drafted the manuscript and contributed to its writing. All authors read and approved the final manuscript.

**Funding**
Not applicable.

**Availibility of data and materials**
Not applicable.

## Declarations

**Competing interests**
The authors declare that they have no competing interests.

Received: 2 May 2022 Accepted: 12 April 2023
Published online: 28 April 2023

**References**

1. Meignan, D., Simonin, O., & Koukam, A. (2007). Simulation and evaluation of urban bus-networks using a multiagent approach. *Simulation Modelling Practice and Theory, 15*, 659–671.
2. Yang, H., Ozbay, K., & Bartin, B. (2010). Application of simulation-based traffic conflict analysis for highway safety evaluation. In *Proceedings of the 12th WCTR, Lisbon (Portugal)*.
3. Barceló, J. (Ed.). (2010). *Fundamentals of traffic simulation. International series in operations research & management science*. Springer.
4. Dowling, R., Skabardonis, A., Alexiadis, V., Wunderlich, K., Vasudevan, M., & Wang, P. (2019). Traffic analysis toolbox volume III: Guidelines for applying traffic microsimulation modeling software 2019. Update to the 2004 Version. Technical report, U.S. Department of Transportation, Federal Highway Administration, Office of Operations. Publication number: FHWA-HOP-18-036.
5. Mansourianfar, M. H., & Haghshenas, H. (2018). Micro-scale sustainability assessment of infrastructure projects on urban transportation systems: Case study of Azadi district, Isfahan Iran. *Cities, 72*, 149–159.
6. Muñoz, J. C., & Daganzo, C. F. (2002). The bottleneck mechanism of a freeway diverge. *Transportation Research Part A: Policy and Practice, 36*(6), 483–505.
7. Leclercq, L., Laval, J. A., & Chiabaut, N. (2011). Capacity drops at merges: An endogenous model. *Transportation Research Part B: Methodological, 45*(9), 1302–1313.
8. Oh, S., & Yeo, H. (2012). Estimation of capacity drop in highway merging sections. *Transportation Research Record, 2286*(1), 111–121.
9. Chen, D., & Ahn, S. (2018). Capacity-drop at extended bottlenecks: Merge, diverge, and weave. *Transportation Research Part B: Methodological, 108*, 1–20.
10. Makridis, M., Leclercq, L., Mattas, K., & Ciuffo, B. (2020). The impact of driving homogeneity due to automation and cooperation of vehicles on uphill freeway sections. *European Transport Research Review, 12*(1), 66.
11. Papathanasopoulou, V., & Antoniou, C. (2018). Flexible car-following models for mixed traffic and weak lane-discipline conditions. *European Transport Research Review, 10*(2), 66.
12. Hans, E., & Damas, C. (2019). Évaluation *a priori* des voies réservées au covoiturage sur voies structurantes d'agglomération. Technical report, Centre d'études et d'expertise sur les risques, l'environnement, la mobilité et l'aménagement, Lyon. Retrieved from http://www.cerema.fr/system/files/documents/2019/05/guide_vsa_evaluation_a_priori_des_voies_reservees_au_covoiturage-mai_2019.pdf
13. Marczak, F., Leclercq, L., & Buisson, C. (2015). A macroscopic model for freeway weaving sections. *Computer-Aided Civil and Infrastructure Engineering, 30*, 464–477.
14. Ratrout, N., Rahman, S. M., & Box, K. (2009). A comparative analysis of currently used microscopic and macroscopic traffic simulation software. *The Arabian Journal for Science and Engineering, 34*, 66.
15. van Beinum, A., Broekman, E., Farah, H., Schakel, W., Wegman, F., & Hoogendoorn, S. (2020). Critical assessment of microscopic simulation models for simulating turbulence around motorway ramps. *Journal of Transportation Engineering, Part A: Systems, 146*(2), 66.
16. Brockfeld, E., Kühne, R. D., & Wagner, P. (2004). Calibration and validation of microscopic traffic flow models. *Transportation Research Record, 1876*(1), 62–70.
17. Toshniwal, P., Hanai, M., & Liu, E. S. (2017). Towards a benchmark for the quantitative evaluation of traffic simulators. In *Proceedings of the 2017 ACM SIGSIM conference on principles of advanced discrete simulation* (pp. 259–262). Association for Computing Machinery.
18. Brockfeld, E., Kühne, R. D., Skabardonis, A., & Wagner, P. (2003). Toward benchmarking of microscopic traffic flow models. *Transportation Research Record, 1852*(1), 124–129.
19. Barceló, J. (2014). Issue 5—Appropriate definitions of calibration and validation. In M. Brackstone & V. Punzo (Eds.), *Traffic simulation: Case for guidelines* (vol. JRC885, pp. 55–58). Joint Reserch Centre.
20. Mohammadian, S., Zheng, Z., Haque, M. M., & Bhaskar, A. (2021). Performance of continuum models for realworld traffic flows: Comprehensive benchmarking. *Transportation Research Part B: Methodological, 147*, 132–167.
21. Ranjitkar, P., Nakatsuji, T., & Kawamua, A. (2005). Car-following models: An experiment based benchmarking. *Journal of the Eastern Asia Society for Transportation Studies, 6*, 1582–1596.
22. Oketch, T., & Carrick, M. (2005). Calibration and validation of a micro-simulation model in network analysis. In *Transportation research board 84th annual meeting, Washington, DC, USA*.
23. Kondyli, A., Duret, A., & Elefteriadou, L. (2007). Evaluation of CORSIM and AIMSUN for freeway merging segments under breakdown conditions. In *Transportation research board 86th annual meeting* (p. 25) (Number: 07-2416).
24. Kan, X. D., Xiao, L., Liu, H., Wang, M., Schakel, W. J., Lu, X.-Y., van Arem, B., Shladover, S. E., & Ferlis, R. A. (2019). Cross-comparison and calibration of two microscopic traffic simulation models for complex freeway corridors with dedicated lanes. *Journal of Advanced Transportation, 2019*(6), 66.
25. Hoogendoorn, S. P., Van Zuylen, H. J., Schreuder, M., Gorte, B., & Vosselman, G. (2003). Microscopic traffic data collection by remote sensing. *Transportation Research Record, 1855*(1), 121–128.
26. Hawas, Y. E., & Hameed, M. A. (2009). A multi-stage procedure for validating microscopic traffic simulation models. *Transportation Planning and Technology, 32*(1), 66.
27. Lighthill, M. J., & Whitham, G. B. (1955). On kinematic waves II. A theory of traffic flow on long crowded roads. *Proceedings of the Royal Society of London Series A Mathematical and Physical Sciences, 229*(1178), 317–345.
28. Richards, P. I. (1956). Shock waves on the highway. *Operations Research, 4*(1), 42–51.
29. Punzo, V., & Montanino, M. (2020). A two-level probabilistic approach for validation of stochastic traffic simulations: Impact of drivers' heterogeneity models. *Transportation Research Part C Emerging Technologies, 121*, 66.
30. Jayakrishnan, R., Tsai, W. K., & Chen, A. (1995). A dynamic traffic assignment model with traffic-flow relationships. *Transportation Research Part C: Emerging Technologies, 3*(1), 51–72.
31. Brackstone, M., & McDonald, M. (1999). Car-following: A historical review. *Transportation Research Part F: Traffic Psychology and Behaviour, 2*(4), 181–196.
32. Saifuzzaman, M., & Zheng, Z. (2014). Incorporating human-factors in car-following models: A review of recent developments and research needs. *Transportation Research Part C: Emerging Technologies, 48*, 379–403.
33. Hamdar, S. (2012). Driver behavior modeling. In A. Eskandarian (Ed.), *Handbook of intelligent vehicles* (pp. 537–558). Springer.
34. Wiedemann, R. (1978). Simulation des Straßenverkehrsflusses. In *Proceedings of the Schriftenreihe des Instituts für Verkehrswesen der Universität Karlsruhe, Germany*.

35. Fritzsche, H. (1994). A model for traffic simulation. *Traffic Engineering and Control, 35*(5), 317–321.
36. Andersen, G. J., & Sauer, C. W. (2007). Optical information for car following: The driving by visual angle (DVA) model. *Human Factors, 49*(5), 878–896.
37. Jin, S., Wang, D.-H., Huang, Z.-Y., & Tao, P.-F. (2011). Visual angle model for car-following theory. *Physica A: Statistical Mechanics and its Applications, 390*(11), 1931–1940.
38. van Winsum, W. (1999). The human element in car following models. *Transportation Research Part F: Traffic Psychology and Behaviour, 2*(4), 207–211.
39. Yang, H.-H., & Peng, H. (2010). Development of an errorable car-following driver model. *Vehicle System Dynamics, 48*(6), 751–773.
40. Chandler, R. E., Herman, R., & Montroll, E. W. (1958). Traffic dynamics: Studies in car following. *Operations Research, 6*(2), 165–184.
41. Gazis, D. C., Herman, R., & Rothery, R. W. (1961). Nonlinear follow-the-leader models of traffic flow. *Operations Research, 9*(4), 545–567.
42. Kometani, E., & Sasaki, T. (1959). A safety index for traffic with linear spacing. *Operations Research, 7*(6), 704–720.
43. Gipps, P. (1981). A behavioural car-following model for computer simulation. *Transportation Research Part B: Methodological, 15*(2), 105–111.
44. Bando, M., Hasebe, K., Nakayama, A., Shibata, A., & Sugiyama, Y. (1995). Dynamical model of traffic congestion and numerical simulation. *Physical Review E, 51*(2), 1035–1042.
45. Davis, L. C. (2003). Modifications of the optimal velocity traffic model to include delay due to driver reaction time. *Physica A: Statistical Mechanics and Its Applications, 319*, 557–567.
46. Newell, G. F. (2002). A simplified car-following theory: A lower order model. *Transportation Research Part B: Methodological, 36*(3), 195–205.
47. Marczak, F. (2014). *Observation empirique et modélisation des discontinuités du réseau autoroutier: vers l'estimation des capacités*. Doctoral dissertation, École nationale des travaux publics de l'État. Retrieved from https://tel.archives-ouvertes.fr/tel-01625190/document.
48. Zheng, Z. (2014). Recent developments and research needs in modeling lane changing. *Transportation Research Part B: Methodological, 60*, 16–32.
49. Michaels, R., & Fazio, J. (1989). Driver behavior model of merging. *Transportation Research Record, 1213*, 4–10.
50. Lee, G. (2006). *Modeling gap acceptance at freeway merges*. Master's thesis, Massachusetts Institute of Technology.
51. Ossen, S., & Hoogendoorn, S. P. (2011). Heterogeneity in car-following behavior: Theory and empirics. *Transportation Research Part C: Emerging Technologies, 19*(2), 182–195.
52. Laval, J. A., & Leclercq, L. (2010). A mechanism to describe the formation and propagation of stop-and-go waves in congested freeway traffic. *Philosophical Transactions of the Royal Society A: Mathematical, Physical and Engineering Sciences, 368*(1928), 4519–4541.
53. Chen, D., Ahn, S., Laval, J., & Zheng, Z. (2014). On the periodicity of traffic oscillations and capacity drop: The role of driver characteristics. *Transportation Research Part B: Methodological, 59*, 117–136.
54. Saifuzzaman, M., Zheng, Z., Haque, M. M., & Washington, S. (2017). Understanding the mechanism of traffic hysteresis and traffic oscillations through the change in task difficulty level. *Transportation Research Part B: Methodological, 105*, 523–538.
55. Newell, G. F. (1993). A simplified theory of kinematic waves in highway traffic, part II: Queueing at freeway bottlenecks. *Transportation Research Part B: Methodological, 27*(4), 289–303.
56. Bécarie, C., Ladino, A., & Gacon, F. (2021). *Symuvia*. https://github.com/licit-lab/SymuVia
57. Laval, J. A., & Leclercq, L. (2008). Microscopic modeling of the relaxation phenomenon using a macroscopic lane-changing model. *Transportation Research Part B: Methodological, 42*(6), 511–522.
58. Laval, J. A., & Daganzo, C. F. (2006). Lane-changing in traffic streams. *Transportation Research Part B: Methodological, 40*(3), 251–264.
59. Aimsun. (2021). *Aimsun next 20 user's manual*. Aimsun Next 20.0.3 edition.
60. Barceló, J., & Casas, J. (2005). Dynamic network simulation with AIMSUN. In R. Kitamura & M. Kuwahara (Eds.), *Simulation approaches in transportation analysis: Recent advances and challenges, operations research/computer science interfaces series* (pp. 57–98). Springer.
61. Gipps, P. (1986). A model for the structure of lane-changing decisions. *Transportation Research Part B: Methodological, 20*(5), 403–414.
62. Álvarez López, P., Behrisch, M., Bieker-Walz, L., Erdmann, J., Flötteröd, Y.-P., Hilbrich, R., Lücken, L., Rummel, J., Wagner, P., & Wießner, E. (2018). Microscopic traffic simulation using SUMO. In *The 21st IEEE international conference on intelligent transportation systems*. IEEE.
63. Krauß, S. (1998). *Microscopic modeling of traffic flow: Investigation of collision free vehicle dynamics*. Doctoral dissertation, University of Cologne, Cologne (Germany). Retrieved from https://sumo.dlr.de/pdf/KraussDiss.pdf.
64. Deutsches Zentrum für Luft- und Raumfahrt e.V. (2021). *Eclipse SUMO—Simulation of Urban MObility*.Retrieved October 27, 2017, from https://github.com/eclipse/sumo/blob/b36f348d9fa5045e7c746007409a12dc26174069/src/microsim/cfmodels/MSCFModel_Krauss.cpp
65. Erdmann, J. (2014). Lane-changing model in SUMO. In *Proceedings of the SUMO2014 modeling mobility with open data* (vol. 24, pp. 77–88). Deutsches Zentrum für Luft- und Raumfahrt e.V.
66. Newell, G. (1993). A simplified theory of kinematic waves in highway traffic, part I: General theory. *Transportation Research Part B: Methodological, 27*(4), 281–287.
67. Ancelet, O., & Hans, E. (2020). Voies structurantes d'agglomération. Fonctionnement des accès. Technical report, Centre d'études et d'expertise sur les risques, l'environnement, la mobilité et l'aménagement, Lyon (France). Retrieved from https://www.cerema.fr/fr/centre-ressources/boutique/voies-structurantes-agglomeration-fonctionnement-acces
68. El-Basha, R. H. S., Hassan, Y., & Sayed, T. A. (2007). Modeling freeway diverging behavior on deceleration lanes. *Transportation Research Record, 2012*(1), 30–37. Publisher: SAGE Publications Inc.
69. Martínez, M. P., García, A., & Moreno, A. T. (2011). Traffic microsimulation study to evaluate freeway exit ramps capacity. *Procedia - Social and Behavioral Sciences, 16*, 139–150. Publisher: Elsevier.
70. Rudjanakanoknad, J. (2012). Capacity change mechanism of a diverge bottleneck. *Transportation Research Record, 2278*(1), 21–30. Publisher: SAGE Publications Inc.
71. Marczak, F., & Buisson, C. (2014). Analytical derivation of capacity at diverging junctions. *Transportation Research Record, 2422*(1), 88–95. Publisher: SAGE Publications Inc.
72. Laval, J. A. (2006). Stochastic processes of moving bottlenecks: Approximate formulas for highway capacity. *Transportation Research Record, 1988*, 86–91.
73. Laval, J. A. (2009). Effects of geometric design on freeway capacity: Impacts of truck lane restrictions. *Transportation Research Part B: Methodological, 43*(6), 720–728.
74. Newell, C. (1982). *Applications of queueing theory*. Chapman and Hall.
75. Daganzo, C. F. (1995). The cell transmission model, part II: Network traffic. *Transportation Research Part B: Methodological, 29*(2), 79–93. Publisher: Pergamon.
76. Torné, J. M., Soriguera, F., & Geroliminis, N. (2014). On the consistency of freeway macroscopic merging models. *Transportation Research Record, 2422*(1), 34–41. Publisher: SAGE Publications Inc.
77. Bar-Gera, H., & Ahn, S. (2010). Empirical macroscopic evaluation of freeway merge-ratios. *Transportation Research Part C: Emerging Technologies, 18*(4), 457–470.
78. Reina, P., & Ahn, S. (2015). On macroscopic freeway merge behavior: Estimation of merge ratios using asymmetric lane flow distribution. *Transportation Research Part C: Emerging Technologies, 60*, 24–35.
79. Troutbeck, R. (2002). The performance of uncontrolled merges using a limited priority process. In *Transportation and traffic theory in the 21st century* (pp. 463–482). Taylor, M.A.P.
80. Cassidy, M., & Ahn, S. (2005). Driver turn-taking behavior in congested freeway merges. *Transportation Research Record, 1934*(1), 140–147. Publisher: SAGE Publications Inc.
81. Reina, P., & Ahn, S. (2014). Prediction of merge ratio using lane flow distribution. In *Transportation research board 93rd annual meeting, Washington, DC*. Number: 14-5459.
82. Elefteriadou, L., Roess, R. P., & McShane, W. R. (1995). Probabilistic nature of breakdown at freeway merge junctions. *Transportation Research Record, 1484*, 80–89.
83. Bertini, R., & Leal, M. (2005). Empirical study of traffic features at a freeway lane drop. *Journal of Transportation Engineering, 131*, 66.
84. Marczak, F., Daamen, W., & Buisson, C. (2013). Merging behaviour: Empirical comparison between two sites and new theory development. *Transportation Research Part C: Emerging Technologies, 36*, 530–546.

85. Daganzo, C. F. (2005). A variational formulation of kinematic waves: Basic theory and complex boundary conditions. *Transportation Research Part B: Methodological, 39*(2), 187–196.
86. Cowan, R. J. (1975). Useful headway models. *Transportation Research, 9*(6), 371–375.
87. Brown, M. (1972). Low density traffic streams. *Advances in Applied Probability, 4*(1), 177–192. Publisher: Cambridge University Press.
88. Roy, R., & Saha, P. (2018). Headway distribution models of two-lane roads under mixed traffic conditions: A case study from India. *European Transport Research Review, 10*(1), 1–12.
89. Li, G., & Cheng, J. (2019). Exploring the effects of traffic density on merging behavior. *IEEE Access, 7*, 51608–51619.
90. Storani, F., Di Pace, R., Bruno, F., & Fiori, C. (2021). Analysis and comparison of traffic flow models: A new hybrid traffic flow model vs benchmark models. *European Transport Research Review, 13*(1), 66.

## Publisher's Note